NIH Public Access
Author Manuscript
Anal Chem. Author manuscript; available in PMC 2013 April 05.

Published in final edited form as:
Anal Chem. 2011 November 15; 83(22): 8756–8765. doi:10.1021/ac2022234.

Two New "Protected" Oxyphors for Biological Oximetry: Properties and Application in Tumor Imaging

Tatiana V. Esipova[†], **Alexander Karagodov**[†], **Joann Miller**[‡], **David F. Wilson**[†], **Theresa M. Busch**[‡], and **Sergei A. Vinogradov**[*,†]

[†]Department of Biochemistry and Biophysics, University of Pennsylvania, Philadelphia, Pennsylvania 19104, United States

[‡]Department of Radiation Oncology, University of Pennsylvania, Philadelphia, Pennsylvania 19104, United States

Abstract

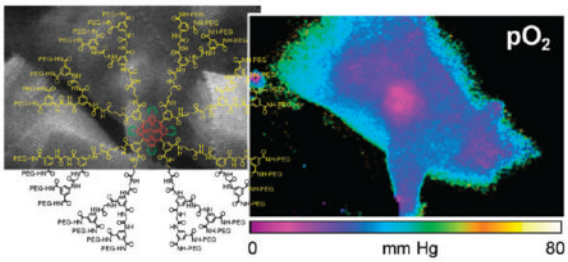

We report the synthesis, calibration, and examples of application of two new phosphorescent probes, Oxyphor R4 and Oxyphor G4, optimized specifically for in vivo oxygen imaging by phosphorescence quenching. These "protected" dendritic probes can operate in either albumin-rich (blood plasma) or albumin-free (interstitial space) environments at all physiological oxygen concentrations, from normoxic to deep hypoxic conditions. Oxyphors R4 and G4 are derived from phosphorescent Pd-*meso*-tetra-(3,5-dicarboxyphenyl)-porphyrin (PdP) or Pd-*meso*-tetra-(3,5-dicarboxyphenyl)-tetrabenzoporphyrin (PdTBP), respectively, and possess features common for protected dendritic probes, i.e., hydrophobic dendritic encapsulation of phosphorescent metalloporphyrins and hydrophilic PEGylated periphery. The new Oxyphors are highly soluble in aqueous environments and do not permeate biological membranes. The probes were calibrated under physiological conditions (pH 6.4–7.8) and temperatures (22–38 °C), showing high stability, reproducibility of signals, and lack of interactions with biological solutes. Oxyphor G4 was used to dynamically image intravascular and interstitial oxygenation in murine tumors in vivo. The physiological relevance of the measurements was demonstrated by dynamically recording changes in tissue oxygenation during application of anesthesia (isofluorane). These experiments revealed that changes in isofluorane concentration significantly affect tissue oxygenation.

The ability to measure changes in tissue oxygenation in real time is of high interest for many branches of physiology and medicine, including neuroscience, ophthalmology, and

© 2011 American Chemical Society

[*]Corresponding Author: vinograd@mail.med.upenn.edu.

ASSOCIATED CONTENT

Supporting Information. Synthetic procedures, ^{1}H and ^{13}C NMR, MALDI-TOF spectra, Stern–Volmer quenching plots, dynamic images of phosphorescence and oxygen (movies), transillumination imaging experiments. This material is available free of charge via the Internet at http://pubs.acs.org.

NIH-PA Author Manuscript
NIH-PA Author Manuscript
NIH-PA Author Manuscript

NIH-PA Author Manuscript

NIH-PA Author Manuscript

NIH-PA Author Manuscript

oncology.[1–4] For example, the development of chronic and fluctuating hypoxic regions in tumors has profound consequences for malignant progression, response to therapy, and patient survival.[2,5,6] Detailed understanding of the biochemical mechanisms of hypoxia tolerance can offer new opportunities for antitumor therapy. In order to conduct such studies, a method for oxygen measurements in tissue in real time is required, which would cause no perturbation of tissue physiology.

Oxygen in biological systems can be measured noninvasively by the phosphorescent quenching method,[7–11] using probes with controllable quenching parameters and defined biodistributions.[12–16] The phosphorescence quenching method relies on the ability of molecular oxygen (O_2) to quench emission of excited triplet state molecules. In biological systems phosphorescence quenching is highly specific to oxygen, since oxygen is the only small-molecule dynamic quencher present in sufficiently high concentration. The dependence of the phosphorescence lifetime (τ) on the partial pressure of oxygen (pO_2) throughout the range of biological concentrations typically follows the Stern–Volmer model (eq 1):

$$1/\tau = 1/\tau_0 + (k_q)(pO_2) \quad (1)$$

where τ is the phosphorescence lifetime at a specified oxygen pressure pO_2, τ_0 is the phosphorescence lifetime in the absence of oxygen ($pO_2 = 0$), and k_q is the quenching constant (see refs 12 and 16 for the outline of the method's principles).

Among the attractive features of the phosphorescence quenching technique are its high specificity, submillisecond temporal response, high sensitivity, and relative simplicity of instrumentation. When soluble probes are used the calibration of the method is absolute in a sense that the probes' quenching parameters must be determined only once and used thereafter for measurements under similar conditions.

A number of oxygen sensing molecules and nanocompositions have been used over the years for different modes of phosphorescence-based oximetry. These include a variety of porphyrinoids,[8,17–22] α-diimine complexes of Ru, Os, Ir, and some other transition metals,[23–27] cyclometalated complexes of Pt, Ir, and Re,[28–33] small-molecule probes supported by polymeric carriers,[34–37] embedded into solid nanoparticles (sol–gel,[38,39] silica,[40,41] polymeric,[42–49] lipobeads[50]) and membrane carriers, such as liposomes[51–53] or polymersomes.[54] Generally, nanoparticle-based materials are suitable for oxygen measurements *in* cell cultures, whereas for the measurements in intact organisms (tissue in vivo), where aqueous solubility and well-defined bio-distributions are particularly important, molecular sensors are the preferred choice. Some examples of in vivo oxygen imaging with nanoparticles have been published.[55]

The original phosphorescent probes, based on simple Pd porphyrins,[8,17,22] required prebinding to macromolecular carriers (e.g., albumin) in order to enhance their aqueous solubility and bring their quenching parameters (τ_0 and k_q, eq 1) into the range compatible with physiological oxygen concentrations (see ref 16 for discussion). However, foreign albumin was a potential source of toxicity and immunogenic responses. Introduction of polyglutamic dendritic porphyrins,[34,56,57] known as Oxyphors R2 and G2,[58] offered a partial solution to this problem. Poly-glutamic probes have high intrinsic aqueous solubility and can be introduced into the blood directly without prebinding to albumin. When in the blood, they form complexes with endogenous albumin, and these complexes serve as ultimate oxygen sensors. As a result, use of R2 and G2 is limited to albumin-rich environments, such as blood plasma (>2% in albumin by weight); but even in such environments, incomplete binding to albumin, which can be easily encountered at higher

NIH-PA Author Manuscript

NIH-PA Author Manuscript

NIH-PA Author Manuscript

probe concentrations (e.g., above ~10^{-5} M), may lead to heterogeneity of the probe signal, skewing the measurement. Notably, combinations of polyglutamic probes with polymeric nanoparticle-based carries have recently been introduced,[47] which alleviate the necessity of albumin binding and allow oxygen measurements in cultured cells.

Recently we disclosed a general approach to protected molecular oxygen probes, which do not require albumin or any other supporting macromolecular carriers or nanocompositions.[12,13,59] In these probes phosphorescent metalloporphyrins are encapsulated inside hydrophobic dendrimers, which form protecting shells, enveloping the chromophores, controlling oxygen diffusion to the excited triplet states, and enabling control over the method's sensitivity. Peripheral PEGylation of the dendrimers ensures high aqueous solubility and prevents interactions of the probes with biological macromolecules.

Here we present synthesis and detailed characterization of two new probes, Oxyphors R4 and G4, intended for wide use in biological research. These probes are built according to the outlined above general scheme; however, their structural elements are further optimized for improved yield of synthesis, higher mono-dispersity, lack of aggregation in aqueous solutions, and overall better chemical stability. One of the probes, Oxyphor G4 was applied to imaging of oxygen distributions in tumors, both intra-vascularly and in the interstitial space. The probe allowed dynamic visualization of the tissue pO_2 levels in the tumor and in the surrounding muscle, as oxygenation responded to changes in the depth of anesthesia. The phosphorescence from the probe also could be detected in transillumination geometry, i.e., through the whole body of the animal, thus demonstrating feasibility of in vivo full body oxygen tomography.

EXPERIMENTAL SECTION

For description of synthesis, instrumentation, and general methods see the Supporting Information.

Phosphorescence Measurements

Dynamic phosphorescence measurements were performed using a PMOD5000 fiber-optic phosphorometer (Oxygen Enterprises), modified in house for time-domain operation. This modification was made possible by using high-power light-emitting diodes (LEDs) (3 W, Lumi-LED, Phillips) as pulsed excitation sources (ca. 10^{-9} s rise time). The detector was an APD module (ca. 3 μs response time, Hamamatsu). The LED current was controlled by a multichannel DAQ NI-6052E board (333 kHz, 16-bit, National Instruments), and the same board was used to digitize the APD output. The LED light and the phosphorescence emission were cleaned up by appropriate cutoff filters (Asahi Spectra). Typically, the excitation pulse was ca. 5 μs long, and the decay was collected during 3–4 ms period after the pulse. The 50–200 decays were averaged for a single lifetime measurement. The decays were analyzed on the fly by the nonlinear least-squares method, implemented as the Marquardt–Levenberg algorithm.[60] The instrument control and the data analysis were performed by a program written in C/C++ (Qt, Nokia).

The calibration setup used in this work was based on the instrumentation described earlier[61] (see the Supporting Information, p S9, for details).

In Vivo Imaging

In vivo oxygen measurements and imaging were performed on tumor-bearing mice, subjected to changes in the depth of anesthesia. Mice were anesthetized by inhalation of isoflurane, admixed to medical air, delivered through a nose cone (VetEquip anesthesia machine, Pleasanton, CA). Depth of anesthesia was altered by changing the percent of

NIH-PA Author Manuscript

NIH-PA Author Manuscript

NIH-PA Author Manuscript

isoflurane between 1.75% and 4.5% at the concentrations and intervals noted in the Results and Discussion. Oxyphor G4 was injected systemically immediately before anesthesia by an intravascular injection (0.01–0.02 mL via the tail vein at the indicated concentration). Alternatively, the probe was injected locally by interstitial injection (0.02–0.03 mL at the indicated concentration) just after induction of the anesthesia. Tumor models included the murine radiation-induced fibrosarcoma (RIF) and human tumor xeno-grafts of non-small-cell lung carcinoma (H460). RIF and H460 tumors were propagated on 9–11 week old C3H or nude mice (NCI-Frederick, Frederick, MD), respectively, by the intradermal injection of 3×10^5 (RIF) or 1×10^6 (H460) cells from in vitro maintained stocks. Phosphorescence lifetime measurements were conducted ~10 days later after the tumors reached the size of ca. 7 mm in diameter.

Local “point” oxygen measurements were performed using the same phosphorometer as in the calibration setup (see above). The light was conducted to and from the animal by a bifurcated quartz optical fiber (Dollan-Jenner).

Phosphorescence lifetime imaging (PLI) was performed in wide-field using a macroscope system. This system is based on an ICCD camera (8-bit) with internal intensifier (Xybion), equipped with a macrozoom lens and a long-pass filter (750 nm cutoff) for optimal collection of phosphorescence. The intensifier on–off time is ca. 10^{-8} s. The excitation source was a PhlatLight LED (Luminous Devices, λ_{max} = 635 nm, 5 W, ca. 10^{-9} s rise time), whose power supply was digitally controlled by an NI-6052E board (National Instruments, 333 kHz clock frequency). The board initiated an excitation pulse of preselected duration upon receiving a TTL trigger from a multichannel counter–timer board KPCI-3140 (Keithly, 40 MHz clock frequency), which served as a main synchronizing unit for the experiment. The digital image acquisition was performed by a frame-grabber board PIXCI-SV5 (Epix), which was timed by the same counter–timer.

The system operated in time domain, whereby the phosphorescence lifetime image (I_τ) was obtained from a series of phosphorescence intensity images (I_n), collected at different delays (δt_n) after the excitation pulse. To obtain a series of images (I_n), the intensifier gate was first opened after a preselected delay δt_1 (usually 10 μs) after the falling edge of the excitation pulse, and image I_1 was acquired on the CCD during a preselected time T, after which the intensifier gate was closed and the image was digitized and stored on the disk. Time T was chosen to allow the phosphorescence to decay completely (usually $5\tau_0$–$10\tau_0$, i.e., 2–3 ms), where τ_0 is defined as in eq 1. Next, the excitation pulse was repeated, and the phosphorescence was acquired beginning with delay δt_2, then with delay δt_3, and so on. The delays δt_n were spaced logarithmically for optimal calculation of the phosphorescence decay times. Fitting of the images I_n with exponentials in each pixel produced the lifetime image I_τ, which was converted into the oxygen pressure map I_{O2} using eq 1. Additionally, the extrapolated image of the phosphorescence initial intensity I_0 (immediately at the end of the excitation pulse) was calculated. In the case when the excitation pulse is much shorter than the phosphorescence decay and all areas in the image receive the same dose of the excitation light—the conditions typically met in our experiments—the image I_0 is proportional to the distribution of the phosphorescent probe, thus providing additional useful information.

RESULTS AND DISCUSSION

Probe Structure and Synthesis

The chemical structures of Oxyphors R4 and G4 are shown in Figure 1, and the complete description of the synthesis can be found in the Supporting Information, p S4.

NIH-PA Author Manuscript

NIH-PA Author Manuscript

NIH-PA Author Manuscript

The phosphorescent cores of porphyrin–dendrimers R4 and G4 comprise Pd-*meso*-tetra-(3,5-dicarboxyphenyl)porphyrin or Pd-*meso*-tetra-(3,5-dicarboxyphenyl)tetrabenzoporphyrin, respectively. Pd tetraarylporphyrins (PdP) have been used as oxygen probes from the onset of the phosphorescence quenching method.[8,9] They possess relatively strong absorption bands in the visible range near 520–530 nm (Q-band, $\varepsilon(\lambda_{max}) \sim 20\ 000\ M^{-1}\ cm^{-1}$) and permit excitation by a variety of sources, including frequency-doubled Nd:YAG lasers (532 nm). On the other hand, Pd tetrabenzoporphyrins (PdTBP) have been developed specifically for oxygen imaging at increased depth in tissue,[17,62] ensured by their strong red-absorbing Q-bands ($\varepsilon(\lambda_{max}) \sim 10^5\ M^{-1}\ cm^{-1}$). Overall, TBP-based probes are better suited for in vivo experiments, as they possess higher molecular extinction coefficients than regular porphyrins and comparable quantum yields. Nonetheless, it is the availability of suitable excitation sources and detectors that often dictates which probe is optimal for a given experiment, and in this sense, PdP-based probes complement near-infrared PdTBP-based molecules.[63,64]

It should be mentioned that today phosphorescent porphyrin complexes with bands spanning practically the entire optical spectrum have become accessible.[12] Aromatic π-extension of the tetrapyrrolic core, originally used to construct phosphorescent metalloporphyrins with symmetrical tetrabenzo- and tetra-naphtho-skeletons,[65–67] also gives rise to macrocycles with different numbers of fused benzo- and naptho-substituents and combinations thereof.[68] Furthermore, fine-tuning of the absorption is possible by varying the metal in a given porphyrin from Pd to Pt. Pt porphyrins have their principal absorption Q-bands typically 10–20 nm blue-shifted relative to those of Pd porphyrins,[69,70] higher phosphorescence quantum yields, and shorter triplet lifetimes. A family of dendritic oxygen probes based on Pt porphyrins has been recently disclosed,[12] and the general design features for Oxyphors R4 and G4 are directly transferable to their Pt analogues.

To prevent aggregation of Pd porphyrins and their interactions with hydrophobic components of biological systems and, at the same time, to tune the quenching rate constants,[61] core elements in both R4 and G4 are encapsulated inside Gen 2 poly-(arylglycine) (AG^2) dendrimers.[71] Attachment of several bulky dendrons to a single porphyrin core unit is challenging because of the unfavorable steric effects. Even though neighboring anchor points (i.e., carboxyls) in the meso-aryl rings are located on the opposite sides of the porphyrin plane, they are still in a close proximity of each other, and that negatively affects their reactivity. A noticeable improvement was achieved by attaching flexible 4-aminobutyrate linkages and thereby moving the anchor sites further apart. According to the matrix-assisted laser desorption ionization time-of-flight (MALDI-TOF) and NMR analyses, attachment of NH_2–AG^2OBu dendrons (for abbreviations see the Supporting Information or ref 12) to aminobutyrate-extended porphyrins was complete, and pure octa-substituted porphyrin–dendrimers were obtained in good yields (73% for R4 and 74% for G4). In comparison, similar structures based on porphyrins without extension arms were typically isolated as mixtures of compounds containing six, seven, and eight dendrons per porphyrin core.[12]

The terminal carboxyl groups of the dendrimers were modified with monomethoxy-poly(ethylene glycol) amines (PEG–NH_2, av MW 1000 Da), which have on average 21–22 (CH_2-CH_2O)– units. Use of long-chain PEG-amines, as opposed to shorter monomethoxy-PEGs (MW 350),[12] constitutes another improvement compared to the earlier reported PEGylated probes. First, amide linkages are much more stable than ester bonds with respect to the hydrolytic cleavage. Second, probes with longer PEG chains have much lesser tendency to aggregation in aqueous solutions than previously disclosed PEGylated AG dendrimers (vide infra).

NIH-PA Author Manuscript

NIH-PA Author Manuscript

NIH-PA Author Manuscript

The molecular weights of the final dendrimers were found to be in the range of ~26 000–44 000 Da with maxima at 35 150 Da for R4 and 35 354 Da for G4. The approximate contents of the PEG residues per dendrimer were determined by rationing the integrated intensities of the peaks, corresponding to the terminal–OMe groups (~3.3 ppm) and methylene protons of 4-amino-butyrate linkages (~1.9 and 2.3 ppm), in the ^{1}H NMR spectra. The average number of the PEG residues per dendrimer was found to be 29 (vs theoretical 32). These data are in good agreement with molecular weights obtained by the MALDI analysis. Overall, the purity of both R4 and G4 compounds was found substantially improved over that of the earlier reported dendritic probes.

The syntheses of R4 and G4 were repeated several times to ensure reproducibility. Both core porphyrins and AG-dendrons can be generated in several gram quantities in a single preparation. Coupling of dendrons to the porphyrins, followed by the hydrolysis of the terminal butyl ester groups and the subsequent PEGylation, also can be performed on a multigram scale. The overall quantities of the probes that can be produced in a single run are limited only by the capacity of chromatographic columns, especially for size exclusion chromatography (SEC), which is required for purification of the final products. Approximately 0.5 g of R4 or G4 can be purified in a single run on a Ø 6 cm × 90 cm column, using Biorad SX-1 beads and THF as a solvent.

Photophysical Properties

The photophysical data for the probes are summarized in Table 1. Both Oxyphors exhibit high solubility and do not aggregate in aqueous solutions, as evidenced by their absorption spectra (Figure 2). No spectral line broadening was observed for either of the probes, and the spectra basically matched those of the parent Pd porphyrins (taken as octacarboxylic acids) in THF or DMF (Supporting Information, p S10). In contrast, the earlier reported Pt and Pd porphyrin–dendrimers, terminated with shorter PEG chains,[12,59] revealed considerable aggregation, manifested by broader absorption bands with shoulders. Longer PEG chains in R4 and G4 are significantly more effective in preventing hydrophobic AG dendrimers from intermolecular association and interactions with other solutes.

The phosphorescence maxima of R4 and G4 in aqueous solutions are located at 698 and 813 nm, respectively, and the phosphorescence spectra exhibit no excitation wavelength dependence. The phosphorescence quantum yields were measured in deoxygenated aqueous solutions (phosphate buffer, pH 7.2, 22°C) relative to the fluorescence of rhodamine 6G (Rh6G) in EtOH (φ_{fl} = 0.94) and found to be 0.037 and 0.017 for R4 and G4, respectively. Notably, when measured against the fluorescence of free-base tetraphenylporphyrin (H_2TPP), a commonly used standard in porphyrin spectroscopy,[72] the quantum yields of the probes were ca. 2 times higher. Apparently, the quantum yield of H_2TPP is only 0.05–0.06 when measured against Rh6G, whereas the commonly used value is 0.11.[72]

Both the absorption Q-band of G4 ($\varepsilon \sim 10^5$ M^{-1} cm^{-1}) and the phosphorescence emission (Figure 1) occur in the red spectral region, where the absorption of endogenous tissue chromophores is significantly diminished.[73] This makes G4 suitable for oxygen measurements at increased depths in the tissue and suggests its potential suitability for deep tissue oxygen tomography.[74]

Oxygen Quenching Properties: Probe Calibration

The oxygen quenching properties of Oxyphors R4 and G4 were measured as functions of concentration, temperature, pH, and presence of biomacromolecules (bovine serum albumin). The measurements were performed in the temperature range of 22–38 °C and pH range of 6.4–7.8 (see the Experimental Section for details).

NIH-PA Author Manuscript

NIH-PA Author Manuscript

NIH-PA Author Manuscript

It is important to mention that because macromolecular probes exist in solutions in multiple conformations, one inherently deals with distributions of phosphorescence lifetimes, as opposed to decays composed of one or more discrete exponentials. For nearly monodisperse dendritic probes, such as R4 and G4, these distributions are quite narrow, and hence, the decays are close to single-exponential. Nevertheless, the only rigorous way to describe such decays is to perform complete phosphorescence lifetime distribution analysis.[76] Lifetime distributions, recovered by the maximum entropy method (MEM) from phosphorescence decays of R4 at three different oxygen concentrations, are shown in Figure 3, as examples.

In addition to the main components, all three decays contain shorter-decaying fractions, although relative contributions of the latter do not exceed 10%. In the case of the air-saturated probe solution, the short-lifetime fraction could not be separated from the main distribution peak (79 μs max), but it can be seen as a shoulder instead. These MEM-recovered histograms are the most probable estimates of the underlying lifetime distributions,[77] and using more conventional fitting with discrete exponentials such decays will be well-approximated by double-exponential fits.

Performing a complete distribution analysis for every decay is computationally expensive and not justified for routine oxygen measurements. Instead, it is appropriate to use "apparent" phosphorescence lifetimes, which are weighted averages derived from the underlying distributions. Averaging can be done in variety of ways: for example, by fitting the data with a double- or triple-exponential function for better residuals, and calculating the intensity or integral-weighted averages. Alternatively, one can enforce single-exponential fitting, neglecting poor residuals and taking advantage of more robust parameter estimation, and use the obtained lifetime as another kind of weighted average. Similarly, measuring the lifetime in frequency domain would produce yet another form of averaging. In this work, to construct Stern–Volmer oxygen quenching plots we used time domain approach and analyzed the decays using either single-exponential or double-exponential fits with integral-weighted averaging. The difference between the Stern–Volmer plots obtained using these two types of apparent lifetimes was found to be minimal (Supporting Information, p S11). In the tables and graphs below the constants (k_q and τ_0) are reported as calculated using single-exponential fitting.

Oxyphor R4

As expected, both k_q and τ_0 of Oxyphor R4 (Figure 4, parts a and b) exhibit dependence on temperature. (The complete titration data for Oxyphor R4 can be found in the Supporting Information, Table 1, p S12.) The quenching constant k_q quasi-linearly increases from 67 to 118 $mmHg^{-1}\ s^{-1}$ with the rise in the temperature from 22 to 38 °C, which corresponds to the temperature coefficient of 3.68 $mmHg^{-1}\ s^{-1}\ °C^{-1}$. The life-time τ_0 decreases from 740 to 677 μs in the same temperature range, corresponding to the coefficient of −3.9 $\mu s\ °C^{-1}$.

The dependence of the calibration parameters on pH was measured at 36.5 °C and four different pH values: 6.4, 6.8, 7.2, and 7.8 (Supporting Information, p S13). Within the measurement error the calibration parameters appear to be pH-independent, with average of $k_q = 111\ mmHg^{-1}\ s^{-1}$ and $\tau_0 = 682\ \mu s$.

In order to determine the concentration range of the probe applicability, the initial concentration ($C_{R4} = 10^{-5}$ M) was increased 2×, 5×, and 10× times, and in each case the titration was performed at 36.5 °C and pH 7.21. The obtained results revealed no deviation from the initial Stern–Volmer plot (Supporting Information, p S16), suggesting that at up to the 10^{-4} M concentration probe molecules do not aggregate and/or do not induce self-quenching.

NIH-PA Author Manuscript

NIH-PA Author Manuscript

NIH-PA Author Manuscript

When oxygen measurements are performed in vivo, endogenous biological species can interact with probe molecules, influencing their excited-state decay properties. Such interactions potentially lead to unpredictable changes in the probe calibration constants and may skew oxygen measurements. Albumin, which is present in the blood serum in 2–3% concentration (by weight), is one of the most plausible candidates to participate in such interactions. In our laboratory we have been using BSA as a test-bed macromolecule to determine whether quenching parameters of phosphorescent probes are affected by biological solutes. For example, quenching constants of Oxyphors R2 and G2 decrease by ca. 10–20 times in solutions containing albumin versus albumin-free solutions,[58] and the same is true for nearly all small-molecule triplet probes.[8] Therefore, the goal is to design macromolecular phosphorescent probes which can operate in either album-free or album-rich environments, but whose calibration constants are unaffected by albumin. Working with such probes, one could be confident that in biological systems oxygen readings would be accurate and absolute. Obviously, the effects of small-molecule quenchers of porphyrin triplet states (e.g., H_2O_2, nitric oxide, quinones, thiols, etc.) cannot be modeled using albumin. Fortunately, in biological systems no such quenching species, except for molecular oxygen, are present in the free form in concentrations high enough to affect probe's phosphorescence.

Phosphorescence of Oxyphor R4 (taken in concentration $C_{R4} = 1 \times 10^{-5}$ M, pH 7.21) was measured in the presence of BSA (2% by weight). The obtained data revealed no deviation from the control Stern–Volmer plots, recorded in the absence of albumin (Supporting Information, p S17). The calibration parameters of R4 were also found to be stable in time. No changes in the Stern–Volmer plot were detected upon storing the probe in aqueous solution at room temperature in the dark for over 2 weeks.

Oxyphor G4

verall, the oxygen quenching behavior of Oxyphor G4 was found to be very similar to that of R4, except that the phosphorescence lifetime τ_0 of the former is significantly shorter, e.g., 243 μs at 22.1 °C. (The complete titration data for Oxyphor G4 can be found in the Supporting Information, Table 2, p S14.) The shorter triplet lifetime of G4 is probably due to higher radiative rates of Pd tetrabenzoporphyrins.[78] The values of k_q and τ_0 of G4 are temperature-dependent (Figure 4, parts c and d), with temperature coefficients of 7.8 $mmHg^{-1}\ s^{-1}\ °C^{-1}$ for k_q and −1.51 $\mu s\ °C^{-1}$ for τ_0.

Noteworthy is a higher (ca. 2–3-fold) value of the quenching constant k_q for G4 relative to that of R4 (Figure 4, parts a and c). This difference could be explained in part by a larger size of the PdTBP core and thus its easier accessibility to oxygen. In addition, the oxygen quenching process in the dendritic probes is most likely not purely diffusion-limited so that the electronic structure of the triplet state affects significantly the rate of the reaction within the encounter complex. Oxygen quenching in the dendritic probes occurs predominantly via the triplet–triplet exchange mechanism,[59] whose efficiency depends on the spectral overlap between the porphyrin triplet state and triplet–singlet excitation bands of the O_2 molecule.[79] This overlap is larger in the case of lower-lying triplet states of π-extended tetrapyrroles, such as PdTBP, increasing the energy transfer probability.

No pH dependence of the calibration parameters was observed for G4 in the range of 6.4–7.8 (Supporting Information, p S15). The average values of k_q and τ_0 at 36.5 °C in that range were found to be 296 $mmHg^{-1}\ s^{-1}$ and 222 μs, respectively. Similar to R4, increase in the concentration of G4 up to 10^{-4} M had no effect on its Stern–Volmer quenching plot (Supporting Information, p S16). Likewise, no dependence of the calibration plots on the presence of albumin was detected (Supporting Information, p S17), and the probe's parameters did not change upon prolonged storage.

NIH-PA Author Manuscript

NIH-PA Author Manuscript

NIH-PA Author Manuscript

In Vivo Oxygen Measurements

In order to demonstrate the applicability of the new probes to real systems, we performed three types of experiments.

First, we injected Oxyphor G4 locally into the interstitial space of the leg muscle of a mouse as well as into a subcutaneously grown tumor and followed tissue oxygenation in these two sites over time (for ca. 1 h), while varying the concentration of isofluorane (anesthesia) in the inhaled gas mixture. An example of local point measurements of oxygen in the muscle and in the tumor on the same animal is shown in Figure 5. The measurements were performed using a two-channel fiber-optic phosphorometer (see the Experimental Section). The probe was excited at 635 nm.

These measurements revealed two important points. First, the oxygenation of both the normal muscle and the tumor were found to be strongly influenced by the anesthesia. Increasing the concentration of isofluorane, inhaled by the animal, to high levels (4%) leads to an abrupt decrease in the tissue pO_2. Although generally this phenomenon is recognized,[80,81] quantitative information about effects of anesthesia on tissue oxygenation is very limited, while being extremely important for medical reasons. This approach allows direct noninvasive tissue oxygen measurements, thereby enabling quantitative studies of the effects of anesthesia.

Second, in this case oxygenation of the normal muscle tissue tends to decrease over time, which may be related to the gradual dehydration of the animal under anesthesia. Oxygenation of the tumor, in contrast, increases. This exemplifies the need for real-time, continuous measurements of tumor oxygenation for understanding the responses of individual tumors to drugs and other therapies, in which oxygen is an important parameter.

In the second set of experiments, we injected G4 into a tumor-bearing mouse systemically and imaged in the wide-field intra-vascular oxygenation, both in the normal tissue and in the tumor, over ca. 1 h.

Each phosphorescence lifetime image was calculated from 10 phosphorescence intensity images, collected at different delays after the excitation pulse (see the Experimental Section). The image sequences were acquired every 10 s, and the calculations were performed on the fly. This allowed us to construct real-time phosphorescence movies, which revealed highly dynamic nature of tissue oxygenation (Supporting Information, m1_pO2.avi, m1_I1.avi). The images shown in Figure 6 represent a single snapshot taken approximately 10 min into the experiment. The first intensity image in the sequence (I_1), acquired after delay of 10 μs (Figure 6c), shows that the probe is localized mainly in the blood plasma, as evidenced by the high contrast of large veins running along the sides of the animal body. If the probe leaked out of the vasculature, these veins would not have such a high contrast, and the contrast would progressively decrease with time of observation.

The brightest area in the image I_1 is colocalized with the tumor; however, the high brightness can be either due to low pO_2 or due to higher local probe concentration, or both. The calculated images of the phosphorescence initial intensity at zero-delay I_0 (Figure 6d) and of the phosphorescence lifetime τ (Figure 6e) reveal that the tumor indeed has low oxygen content. The tumor area has significantly longer phosphorescence lifetimes than the surrounding tissue, even though the concentration of the excited-state probe in the tumor is actually below that in the surrounding tissue at the time when this image was acquired, as evidenced by the darker spot in the I_0 image (Figure 6d). Consequently, the oxygen image (Figure 6f) shows the hypoxic tumor area, where the pO_2 values reach 10 mmHg and lower.

NIH-PA Author Manuscript

NIH-PA Author Manuscript

NIH-PA Author Manuscript

Because Oxyphor G4 is nontoxic and is retained in the blood for a long time (hours), the same animal could be imaged on the following day (Supporting Information, p S18). These experiments revealed that some of the probe accumulated in the tumor, presumably in the interstitial space, whereas the most of it cleared out of the vasculature. This probe behavior is consistent with the well-known EPR (enhanced permeability and retention) effect[82] common for many tumor types.

Next, G4 was injected locally into the interstitial space of a tumor as well as into the nearby muscle (similar to the first experiment), and the oxygenation was also imaged dynamically over time (Supporting Information, m2_pO2.avi, m2_I0.avi, m2_I1.avi). This type of imaging is different in a sense that it allows direct visualization of the local interstitial (tissue), as opposed to intravascular, pO_2 distributions. The oxygen images in this case were collected at 0.5 Hz rate, and the phosphorescence movies were constructed to visualize the oxygenation dynamics. Higher frame rate was necessary in this case in order to investigate transient effects of hypoxia, induced by short periods (ca. 10 s) of inhalation of nitrogen.

A snapshot taken ca. 10 min into the experiment is shown in Figure 7. The tumor region (enclosed in a yellow circle, image b of Figure 7) was marked by several black dots on the skin, and the probe injection site outside the tumor area (shown with the left yellow arrow on image b of Figure 7) was also marked. It can be seen that the probe injected in muscle outside of the tumor diffused toward the animal's leg, whereas the solution injected into the tumor remained within the tumor boundaries. Notably, a larger amount of the probe was deliberately injected into the muscle than into the tumor. As in the intravascular imaging experiment (above), the tumor area in this case appears as a hypoxic site (Figure 7f), characterized by significantly longer phosphorescence lifetimes (Figure 7e), but lesser initial intensity I_0 (Figure 7d), which is consistent with a smaller injected amount of the probe. The tissue oxygen pressures responded rapidly to the hypoxic challenge. Interestingly, the muscle tissue near the tumor undergoes marked alterations in oxygen levels over time, including values well below normal (Supporting Information, m2_pO2.avi). Such fluctuations are usually not observed in normal muscle, but have previously been reported to occur in muscle tissues near tumors.[83] This is consistent with effluent blood from the tumor mixing with influent blood for the muscle through inappropriately developed vessel structures.

Finally, we performed transillumination imaging experiments, in which the excitation source (LED) was positioned under the animal body, while the imaging detector was positioned above the animal (Supporting Information, p S19). In this configuration, the excitation light had to diffuse through the entire body of the mouse before reaching the tumor on the opposite side and exciting the phosphorescence in the tumor interstitial space. This experiment demonstrates that phosphorescence detection is possible even when the excitation photons diffuse through the animal body, thereby proving the feasibility of the whole-body tomographic oxygen imaging[74] with Oxyphor G4.

CONCLUSIONS

The two new phosphorescent probes, Oxyphors R4 and G4, are well-characterized dendritic macromolecular compounds, designed specifically for biological oxygen imaging in vivo. Their principal advantage over the previously developed dendritic probes is complete independence of the calibration parameters on the properties of the biological medium. The new probes can be used for measurements in blood plasma or directly in the tissue interstitial space. We speculate that the probes should perform equally well in intracellular imaging, provided appropriate delivery mechanisms into the cell are developed, e.g., inside carrier vesicles.[54] Needless to say, both R4 and G4 are also perfectly suitable for oxygen

NIH-PA Author Manuscript

NIH-PA Author Manuscript

NIH-PA Author Manuscript

measurements in vitro in bulk samples, such as in extracellular media and/or in enzymatic assays.

As illustrated by pilot experiments, Oxyphor G4 makes it possible to longitudinally image interstitial oxygenation in tumors—an extremely important parameter in cancer physiology. In particular, G4 should allow direct noninvasive pO_2 imaging in tumors over the course of delivery of chemotherapy, radiation, or photodynamic therapy (PDT). This ability should shed light on treatment effects on tumor microenvironment with the potential to separate effects within the interstitium from those at the level of the vasculature. Such data can facilitate study of the vascular versus cellular mechanisms of damage by cancer therapeutics, which, among other uses, would inform the introduction of complementary treatment approaches. Particularly advantageous would be the ability to visualize oxygen distributions in tumor tissue in three dimensions (3D), for which combination of G4 with phosphorescence lifetime tomography will be an ideal tool.

Supplementary Material

Refer to Web version on PubMed Central for supplementary material.

Acknowledgments

Support of the Grants EB007279, HL081273, and CA085831 from the NIH U.S.A. is gratefully acknowledged.

References

1. Yu DY, Cringle SJ. Exp Eye Res. 2005; 80:745. [PubMed: 15939030]
2. Tatum JL, Kelloff GJ, Gillies RJ, Arbeit JM, Brown JM, Chao KS, Chapman JD, Eckelman WC, Fyles AW, Giaccia AJ, Hill RP, Koch CJ, Krishna MC, Krohn KA, Lewis JS, Mason RP, Melillo G, Padhani AR, Powis G, Rajendran JG, Reba R, Robinson SP, Semenza GL, Swartz HM, Vaupel P, Yang D, Croft B, Hoffman J, Liu G, Stone H, Sullivan D. Int J Radiat Biol. 2006; 82:699. [PubMed: 17118889]
3. Blomgren K, Hagberg H. Free Radical Biol Med. 2006; 40:388. [PubMed: 16443153]
4. Schreml S, Szeimies RM, Prantl L, Karrer S, Landthaler M, Babilas P. Br J Dermatol. 2010; 163:257. [PubMed: 20394633]
5. Brown JM. J Natl Cancer Inst. 1990; 82:338. [PubMed: 2406450]
6. Semenza GL. Physiology. 2009; 24:97. [PubMed: 19364912]
7. Wilson DF. Am J Physiol: Heart Circ Physiol. 2008; 294:H11. [PubMed: 17993593]
8. Vanderkooi JM, Maniara G, Green TJ, Wilson DF. J Biol Chem. 1987; 262:5476. [PubMed: 3571219]
9. Rumsey WL, Vanderkooi JM, Wilson DF. Science. 1988; 241:1649.
10. Golub AS, Pittman RN. Am J Physiol: Heart Circ Physiol. 2008; 294:H2905. [PubMed: 18375716]
11. Golub AS, Tevald MA, Pittman RN. Am J Physiol: Heart Circ Physiol. 2011; 300:H135. [PubMed: 20971766]
12. Lebedev AY, Cheprakov AV, Sakadzic S, Boas DA, Wilson DF, Vinogradov SA. ACS Appl Mater Interfaces. 2009; 1:1292. [PubMed: 20072726]
13. Finikova OS, Lebedev AY, Aprelev A, Troxler T, Gao F, Garnacho C, Muro S, Hochstrasser RM, Vinogradov SA. Chem-PhysChem. 2008; 9:1673.
14. Sakadžić S, Roussakis E, Yaseen MA, Mandeville ET, Srinivasan VJ, Arai K, Ruvinskaya S, Devor A, Lo EH, Vinogradov SA, Boas DA. Nat Methods. 2010; 7:755. [PubMed: 20693997]
15. Lecoq J, Parpaleix A, Roussakis E, Ducros M, Houssen YG, Vinogradov SA, Charpak S. Nat Med. 2011; 17:893. [PubMed: 21642977]
16. Vinogradov, SA.; Wilson, DF. Designing Dendrimers. Campagna, S.; Ceroni, P.; Puntoriero, F., editors. Wiley; 2011.

NIH-PA Author Manuscript

NIH-PA Author Manuscript

NIH-PA Author Manuscript

17. Vinogradov SA, Wilson DF. J Chem Soc, Perkin Trans. 1995; 2:103.
18. Papkovsky DB, Ponomarev GV, Trettnak W, Oleary P. Anal Chem. 1995; 67:4112.
19. Lee SK, Okura I. Anal Commun. 1997; 34:185.
20. Borisov SM, Papkovsky DB, Ponomarev GV, DeToma AS, Saf R, Klimant I. J Photochem Photobiol, A. 2009; 206:87.
21. Papkovsky DB, Ponomarev GV. Spectrochim Acta, Part A. 2001; 57:1897.
22. Papkovsky DB, O'Riordan TC. J Fluoresc. 2005; 15:569. [PubMed: 16167215]
23. Kalyanasundaram, K. Photochemistry of Polypyridine and Porphyrin Complexes. Academic Press; London: 1992.
24. Castellano FN, Lakowicz JR. J Photochem Photobiol. 1998; 67:179.
25. Zhong W, Urayama P, Mycek MA. J Phys D: Appl Phys. 2003; 36:1689.
26. Fernandez-Sanchez JF, Roth T, Cannas R, Nazeeruddin MK, Spichiger S, Graetzel M, Spichiger-Keller UE. Talanta. 2007; 71:242. [PubMed: 19071295]
27. Xu W, Kneas KA, Demas JN, DeGraff BA. Anal Chem. 1996; 68:2605. [PubMed: 21619207]
28. DeRosa MC, Mosher PJ, Yap GPA, Focsaneanu KS, Crutchley RJ, Evans CEB. Inorg Chem. 2003; 42:4864. [PubMed: 12895108]
29. Borisov SM, Klimant I. Anal Chem. 2007; 79:7501. [PubMed: 17718539]
30. Bronner C, Baudron SA, Hosseini MW, Strassert CA, Guenet A, De Cola L. Dalton Trans. 2010; 39:180. [PubMed: 20023948]
31. Guo HM, Ji SM, Wu WH, Wu WT, Shao JY, Zhao JZ. Analyst. 2010; 135:2832. [PubMed: 20835478]
32. Tseng YH, Bhattacharya D, Lin SM, Thanasekaran P, Wu JY, Lee LW, Sathiyendiran M, Ho ML, Chung MW, Hsu KC, Chou PT, Lu KL. Inorg Chem. 2010; 49:6805. [PubMed: 20614862]
33. Di Marco G, Lanza M, Antonio M, Stefio I, Di Petro C, Romeo G, Campagna S. Anal Chem. 1998; 70:5019. [PubMed: 21644681]
34. Vinogradov SA, Lo LW, Wilson DF. Chem— Eur J. 1999; 5:1338.
35. Briñas RP, Troxler T, Hochstrasser RM, Vinogradov SA. J Am Chem Soc. 2005; 127:11851. [PubMed: 16104764]
36. Dmitriev RI, Zhdanov AV, Ponomarev GV, Yashunski DV, Papkovsky DB. Anal Biochem. 2010; 398:24. [PubMed: 19931212]
37. Gillanders RN, Arzhakova OV, Hempel A, Dolgova A, Kerry JP, Yarysheva LM, Bakeev NF, Volynskii AL, Papkovsky DB. Anal Chem. 2010; 82:466. [PubMed: 20038091]
38. Xu H, Aylott JW, Kopelman R, Miller TJ, Philbert MA. Anal Chem. 2001; 73:4124. [PubMed: 11569801]
39. Blair S, Kataky R, Parker D. New J Chem. 2002; 26:530.
40. Xu H, Zhang Z. Biosens Bioelectron. 2007; 22:2743. [PubMed: 17360175]
41. Zhang HD, Sun YH, Ye KQ, Zhang P, Wang Y. J Mater Chem. 2005; 15:3181.
42. Im SH, Khalil GE, Callis J, Ahn BH, Gouterman M, Xia Y. Talanta. 2005; 67:492. [PubMed: 18970194]
43. Zhang G, Chen J, Payne SJ, Kooi SE, Demas JN, Fraser CL. J Am Chem Soc. 2007; 129:8942. [PubMed: 17608480]
44. Cywinski PJ, Moro AJ, Stanca SE, Biskup C, Mohr GJ. Sens Actuators, B. 2009; B135:472.
45. Borisov SM, Klimant I. Microchim Acta. 2009; 164:7.
46. Wu CF, Bull B, Christensen K, McNeill J. Angew Chem, Int Ed. 2009; 48:2741.
47. Lee YEK, Ulbrich EE, Kim G, Hah H, Strollo C, Fan WZ, Gurjar R, Koo SM, Kopelman R. Anal Chem. 2010; 82:8446. [PubMed: 20849084]
48. Kersey FR, Zhang GQ, Palmer GM, Dewhirst MW, Fraser CL. ACS Nano. 2010; 4:4989. [PubMed: 20704337]
49. Coogan MP, Court JB, Gray VL, Hayes AJ, Lloyd SH, Millet CO, Pope SJA, Lloyd D. Photochem Photobiol Sci. 2010; 9:103. [PubMed: 20062850]
50. Ma A, Rosenzweig Z. Anal Bioanal Chem. 2005; 382:28. [PubMed: 15900448]

NIH-PA Author Manuscript

NIH-PA Author Manuscript

NIH-PA Author Manuscript

51. McNamara KP, Rosenzweig N, Rosenzweig Z. Mikrochim Acta. 1999; 131:57.
52. McNamara KP, Rosenzweig Z. Anal Chem. 1998; 70:4853.
53. Cheng Z, Aspinwall CA. Analyst (Cambridge, UK). 2006; 131:236.
54. Sinks LE, Robbins GP, Roussakis E, Troxler T, Hammer DA, Vinogradov SA. J Phys Chem B. 2010; 114:14373. [PubMed: 20462225]
55. Palmer GM, Fontanella AN, Zhang GQ, Hanna G, Fraser CL, Dewhirst MW. J Biomed Opt. 2010; 15:066021. [PubMed: 21198195]
56. Vinogradov SA, Wilson DF. Adv Exp Med Biol. 1997; 428:657. [PubMed: 9500112]
57. Rietveld IB, Kim E, Vinogradov SA. Tetrahedron. 2003; 59:3821.
58. Dunphy I, Vinogradov SA, Wilson DF. Anal Biochem. 2002; 310:191. [PubMed: 12423638]
59. Ceroni P, Lebedev AY, Marchi E, Yuan M, Esipova TV, Bergamini G, Wilson DF, Busch TM, Vinogradov SA. Photochem Photobiol Sci. 2011; 10:1056. [PubMed: 21409208]
60. Press, WH.; Teukolsky, SA.; Vetterling, WT.; Flannery, BP. Numerical Recepies in C. Cambrdige University Press; Cambridge, U.K: 1992.
61. Rozhkov V, Wilson D, Vinogradov S. Macromolecules. 2002; 35:1991.
62. Vinogradov SA, Lo LW, Jenkins WT, Evans SM, Koch C, Wilson DF. Biophys J. 1996; 70:1609. [PubMed: 8785320]
63. Sakadžić S, Yuan S, Dilekoz E, Ruvinskaya S, Vinogradov SA, Ayata C, Boas DA. Appl Opt. 2009; 48:D169. [PubMed: 19340106]
64. Yaseen MA, Srinivasan VJ, Sakadžić S, Wu W, Ruvinskaya S, Vinogradov SA, Boas DA. Opt Express. 2009; 17:22341. [PubMed: 20052157]
65. Finikova OS, Cheprakov AV, Beletskaya IP, Carroll PJ, Vinogradov SA. J Org Chem. 2004; 69:522. [PubMed: 14725469]
66. Finikova OS, Aleshchenkov SE, Brinas RP, Cheprakov AV, Carroll PJ, Vinogradov SA. J Org Chem. 2005; 70:4617. [PubMed: 15932297]
67. Finikova OS, Cheprakov AV, Vinogradov SA. J Org Chem. 2005; 70:9562. [PubMed: 16268634]
68. Niedermair F, Borisov SM, Zenkl G, Hotmann OT, Weber H, Saf R, Klimant I. Inorg Chem. 2010; 49:9333. [PubMed: 20839844]
69. Eastwood D, Gouterman M. J Mol Spectrosc. 1970; 35:359.
70. Kim DH, Holten D, Gouterman M, Buchler JW. J Am Chem Soc. 1984; 106:4015.
71. Vinogradov SA. Org Lett. 2005; 7:1761. [PubMed: 15844900]
72. Seybold PG, Gouterman M. J Mol Spectrosc. 1969; 31:1.
73. Wang, LV.; Wu, HI. Biomedical Optics. Wiley; New York: 2007.
74. Apreleva SV, Wilson DF, Vinogradov SA. Appl Opt. 2006; 45:8547. [PubMed: 17086268]
75. Kubin RF, Fletcher AN. J Lumin. 1982; 27:455.
76. Vinogradov SA, Wilson DF. Appl Spectrosc. 2000; 54:849.
77. Livesey AK, Brochon JC. Biophys J. 1987; 52:693. [PubMed: 19431708]
78. Lebedev AY, Filatov MA, Cheprakov AV, Vinogradov SA. J Phys Chem A. 2008; 112:7723. [PubMed: 18665576]
79. Ogilby PR. Chem Soc Rev. 2010; 39:3181. [PubMed: 20571680]
80. Swartz HM, Taie S, Miyake M, Grinberg OY, Hou H, el-Kadi H, Dunn JF. Adv Exp Med Biol. 2003; 530:569. [PubMed: 14562753]
81. Ziemer LS, Lee WMF, Vinogradov SA, Sehgal C, Wilson DF. J Appl Physiol. 2005; 98:1503. [PubMed: 15579567]
82. MacEwan SR, Callahan DJ, Chilkoti A. Nanomedicine. 2010; 5:793. [PubMed: 20662649]
83. Cerniglia GJ, Wilson DF, Pawlowski M, Vinogradov S, Biaglow J. J Appl Physiol. 1997; 82:1939. [PubMed: 9173962]

NIH-PA Author Manuscript

NIH-PA Author Manuscript

NIH-PA Author Manuscript

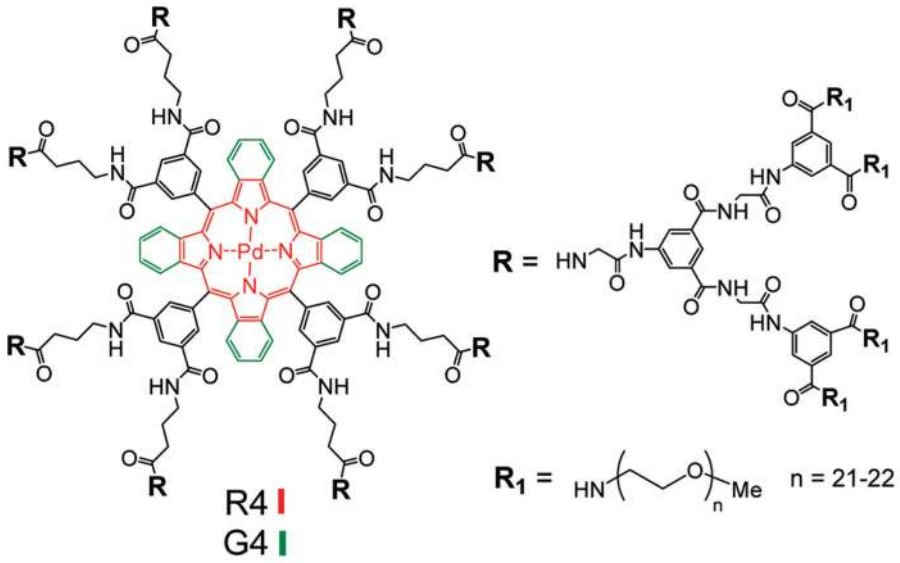

Figure 1.
Structures of Oxyphors R4 and G4 (PEG-amine av MW 1000).

NIH-PA Author Manuscript
NIH-PA Author Manuscript
NIH-PA Author Manuscript

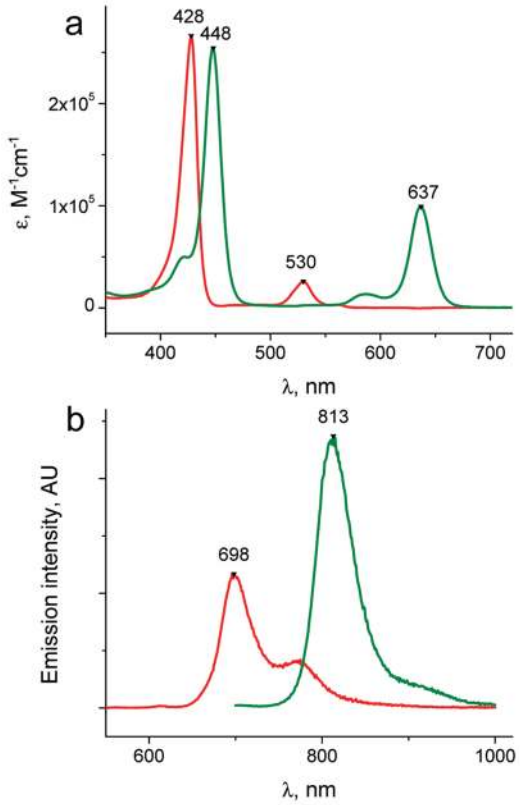

Figure 2.

Absorption (a) and emission (b) spectra of R4 (red) and G4 (green) in 50 mM phosphate buffer solutions (pH 7.2). The emission spectra are scaled by the brightness indexes (*B*) of the probes at zero-oxygen concentration. Brightness (*B*) is defined as a product of the molar extinction coefficient ε and the phosphorescence quantum yield φ ($B = \varepsilon\varphi$).

NIH-PA Author Manuscript

NIH-PA Author Manuscript

NIH-PA Author Manuscript

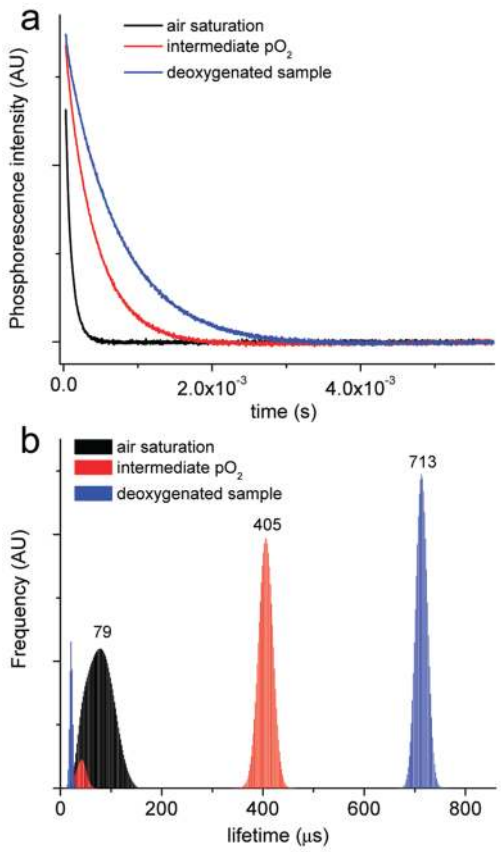

Figure 3.

Phosphorescence decays (a) of probe Oxyphor R4 recorded at three different oxygen concentrations (air saturation, intermediate pO_2, deoxygenated) from 10 μM buffered solutions at 22.5 °C (phosphate buffer, 50 mM, pH 7.2). Phosphorescence was excited by 5 μs long LED pulses. Phosphorescence lifetime distributions (b) recovered by the maximum entropy method (MEM) (ref 76).

NIH-PA Author Manuscript

NIH-PA Author Manuscript

NIH-PA Author Manuscript

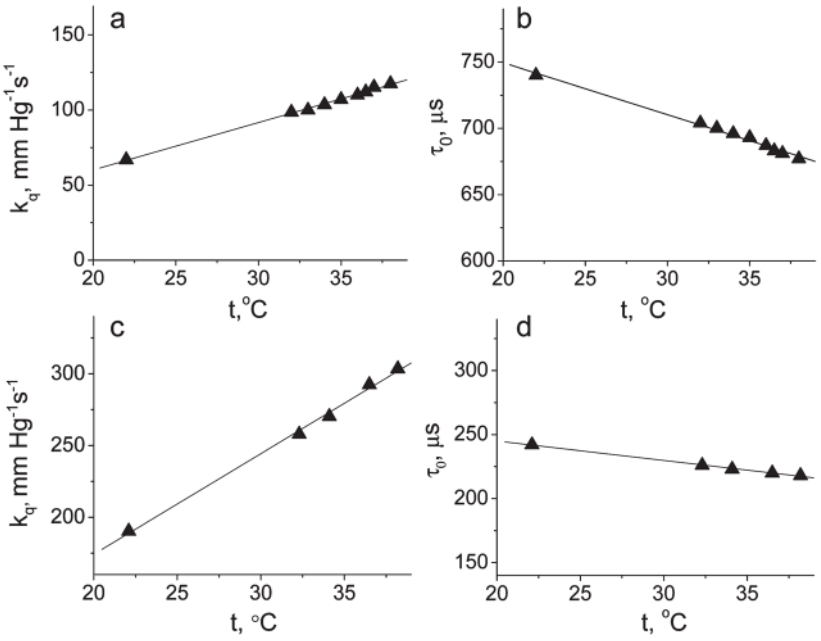

Figure 4.

Temperature dependencies of oxygen quenching constants (k_q) and lifetimes (τ_0) for Oxyphors R4 (a and b) and G4 (c and d). The measurements were performed using 10 μM solutions of the probes in 50 mM phosphate buffer, pH 7.2.

NIH-PA Author Manuscript

NIH-PA Author Manuscript

NIH-PA Author Manuscript

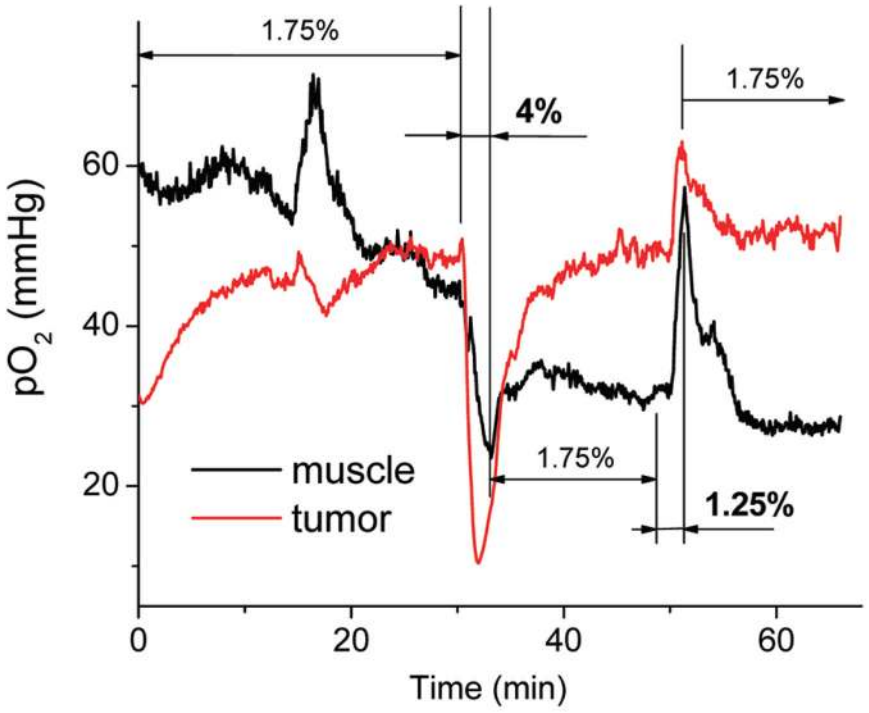

Figure 5.

Changes in interstitial (tissue) oxygenation in the leg muscle and in subcutaneous tumor (RIF) in a C3H mouse, as measured using Oxyphor G4 and a fiber-optic phosphorometer. Solution of G4 (20 μL, 10 μM) in physiological saline was injected directly into the tissue. Measurements were performed at 4 s intervals. The anesthetic gas mixture was delivered at the rate of 2 L/min, and the normal concentration of isofluorane in the mixture (1.75%) was changed briefly by higher (4%) or lower (1.25%) levels.

NIH-PA Author Manuscript

NIH-PA Author Manuscript

NIH-PA Author Manuscript

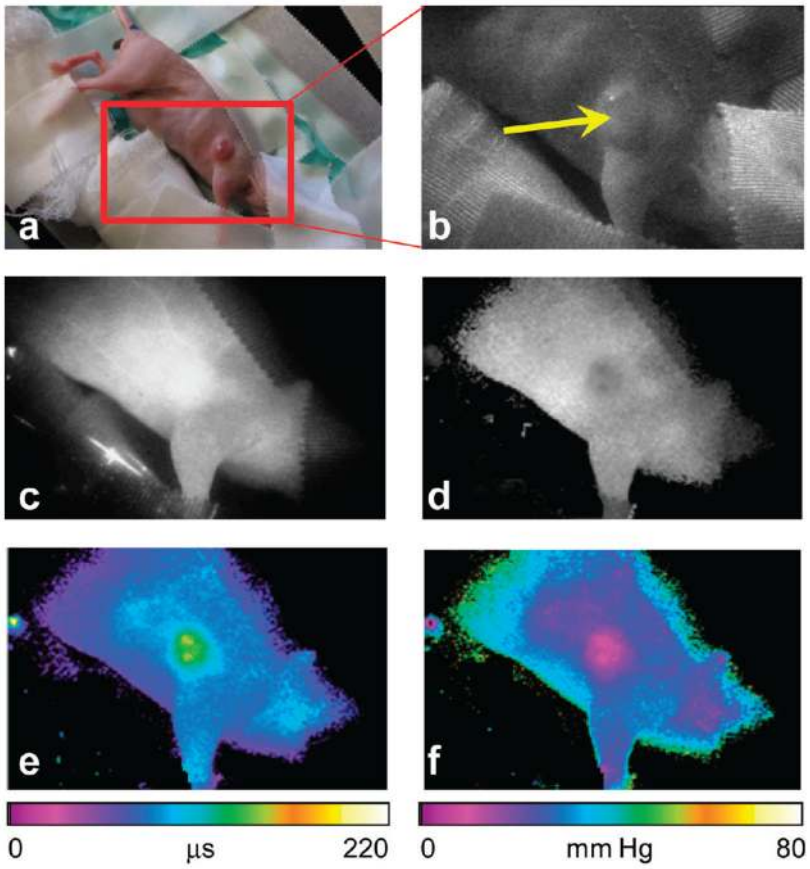

Figure 6.

Imaging of intravascular oxygenation in a mouse using Oxyphor G4. The probe was injected via the tail vein to achieve the final concentration in the blood plasma of ca. 4 μM. (a) Photograph of the anesthetized animal on a heating pad and (b) the zoomed-in region, as imaged by the ICCD camera. The tumor is located on the right shoulder of the animal (pointed by yellow arrow). (c) Image (I_1) of the phosphorescence intensity acquired after delay δt_1 = 10 μs, following the excitation pulse. In total, 10 images at different delays, from 10 to 620 μs, were collected. Calculated images of (d) phosphorescence initial intensity (I_0), (e) phosphorescence lifetimes (τ, color scale in μs), and (f) partial oxygen pressure (pO_2, color scale in mm Hg).

NIH-PA Author Manuscript

NIH-PA Author Manuscript

NIH-PA Author Manuscript

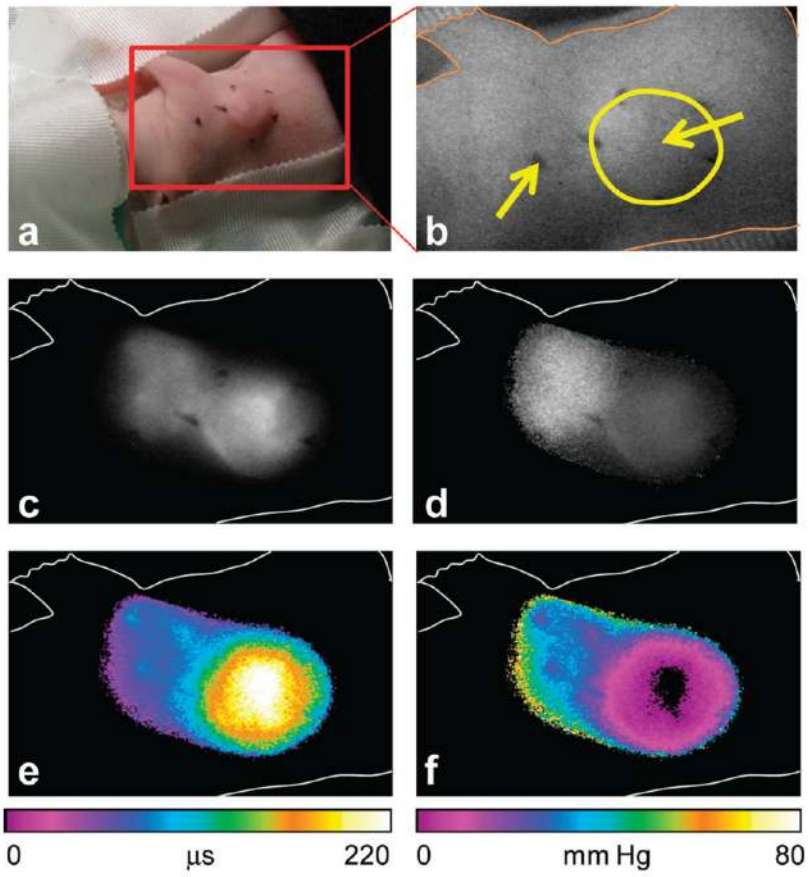

Figure 7.

Imaging of interstitial (pericellular space) oxygenation using Oxyphor G4. The probe (20 μM solution) was injected directly into the normal (40 μL) and tumor (20 μL) tissue. (a) Photograph of the anesthetized animal on a heating pad and (b) the zoomed-in region, as imaged by the ICCD camera. The tumor is located on the right shoulder of the animal (enclosed in a yellow circle), and the probe injection sites are marked by the arrows. (c) Image (I_1) of the phosphorescence intensity acquired after delay of 10 μs, following the excitation pulse. Calculated images of (d) phosphorescence initial intensity (I_0), (e) phosphorescence lifetimes (τ, color scale in μs), and (f) partial oxygen pressure (pO_2, color scale in mm Hg). To simplify visualization, the contours of the animal body (as in image b) are shown in images c–f.

NIH-PA Author Manuscript

NIH-PA Author Manuscript

NIH-PA Author Manuscript

Table 1

Photophysical Properties of Oxyphors R4 and G4

probe	absorption, nm ($\varepsilon \times 10^{-4}$, M^{-1} cm^{-1})[a]	emission λ_{max}, nm	φ/τ_0, μs[b]
R4	428 (26.7 ± 0.4)	698	0.037[c]/733 (0.073)[d]
	530 (2.55 ± 0.08)		
G4	448 (25.4 ± 0.9)	813	0.017[c]/242 (0.033)[d]
	637 (9.9 ± 0.4)		

[a]The extinction coefficients were determined using 50 mM phosphate buffer solutions (pH 7.2), assuming the molecular weights of 35 151 Da for R4 and 35 374 Da for G4. These molecular weights correspond to the distribution maxima in the MALDI-TOF spectra.

[b]The emission spectra were recorded in 50 mM phosphate buffer (pH 7.2) solutions, deoxygenated by Ar.

[c]The quantum yields were determined relative to the fluorescence of Rh6G (φ_{fl} = 0.94) in EtOH (ref 75).

[d]The quantum yields were determined relative to the fluorescence of H_2TPP (φ_{fl} = 0.11) in deoxygenated benzene (ref 72).